# Terahertz plasmonics

N. Yu, Q.J. Wang, M.A. Kats, J.A. Fan, F. Capasso,
S.P. Khanna, L. Li, A.G. Davies and E.H. Linfield

Semiconductor microstructures can be used to tailor the dispersion properties of surface plasmon polaritons in the terahertz (THz) frequency range, and therefore can be used as important building blocks for terahertz optical devices. The physical principles of three structures are discussed: plasmonic second-order gratings, designer (spoof) surface plasmon polariton structures, and channel polariton structures. The effectiveness of these structures is demonstrated by utilising them to improve power throughput and to reduce the beam divergence of edge-emitting THz quantum cascade lasers. Plasmonics promises compact and low-loss solutions for manipulating light at THz wavelengths, and will have a large impact on applications such as imaging, light detection and ranging (LIDAR), and the heterodyne detection of chemicals.

*Introduction:* Plasmonics involves manipulation of surface plasmon polaritons (SPPs), which are collective oscillations of electrons on the surface of a metal interacting with electromagnetic fields [1–6]. Localised SPPs generate significantly enhanced optical near fields when light is scattered by small metallic particles, a problem systematically treated by Mie in 1908 [7]. SPPs also exist on a planar interface between a metal and a dielectric as electron density waves coupled to electromagnetic waves. In 1907, Zenneck studied a similar problem: the propagation of radio waves on the surface of the Earth [8].

In contrast to conventional optical components, plasmonic structures can manipulate light at a subwavelength scale. This is due to the large spatial frequency components associated with metallic structures with subwavelength-sharp features. SPPs have been intensively studied in the last two decades, but the focus has been primarily on the visible and near-infrared regimes [4–6]. In dealing with terahertz (THz) or even lower frequency radiation, the following question arises: are there 'real' surface plasmons at such long wavelengths? By 'real' we mean having the key property of strong (i.e. subwavelength) confinement typical of surface plasmons at visible and near-infrared frequencies.

It is known that the in-plane wavevector of SPPs on a planar interface is [1–6]

$$\beta(\omega) = k_o\sqrt{\varepsilon_d\varepsilon_m(\omega)/(\varepsilon_d + \varepsilon_m(\omega))} \quad (1)$$

where $\varepsilon_d$ and $\varepsilon_m$ are, respectively, the complex permittivity of the dielectric and metal defining the interface, and $k_o$ is the vacuum wavevector. While $\varepsilon_d$ is, in general, weakly dependent on $\omega$ away from the restrahlen bands, $\varepsilon_m$ is strongly dispersive. As such, the in-plane wavevector $\beta$ departs from $k_o\sqrt{\varepsilon_d}$ as $\omega$ increases and the deviation reaches a maximum when the real part of $\varepsilon_m$ is negative and has an absolute value equal to $\varepsilon_d$ (i.e. the absolute value of the denominator in (1) is minimised). The frequency at which this condition is satisfied is called the asymptotic SPP frequency; it is usually in the visible or ultraviolet for common metals such as Au, Ag, Cu, Al, etc. At THz frequencies, however, the real part of $\varepsilon_m$ is at least two to three orders of magnitude greater than that of $\varepsilon_d$ so that the SPP dispersion curve is well approximated by the light line: $\beta(\omega) \simeq k_o\sqrt{\varepsilon_d}$. As a result, the out-of-plane wavevector (i.e. the decay rate normal to the interface)

$$|\kappa| = \sqrt{\beta^2 - k_o^2\varepsilon_d} \quad (2)$$

is very small, corresponding to poorly confined surface waves, known as Sommerfeld or Zenneck waves [8–10]. In this regard, there are no surface plasmons in the real sense at THz frequencies. Note that in this Letter we identify two regimes of SPPs: 'surface plasmons' refer to SPPs near the asymptote of the dispersion curve, while 'Zenneck waves' correspond to SPPs at the low-frequency end of the dispersion curve.

*Engineering dispersion of THz surface waves using plasmonics:* The above picture is changed completely by microstructuring the metallic surfaces. The simplest example is a metallic surface patterned with a Bragg grating with periodicity $\Lambda$. Like electron waves interacting with a periodic potential or light waves interacting with a photonic crystal, SPPs with certain frequencies experience strong Bragg reflections from the grating so that they are forbidden to propagate [11–14]. In the dispersion diagram, small bandgaps open up in the vicinity of $\beta = m\pi/\Lambda$, $m$ being an integer. Assuming we operate in a region close to one of these bandgaps where $\beta$ deviates from the light line (Fig. 1), the confinement of SPPs, according to (2), will be significantly improved and we recover the surface plasmon regime. We will see later that plasmonic collimators based on $\beta \simeq 2\pi/\Lambda$ (i.e. second-order gratings) can successfully shape the output of THz quantum cascade lasers (QCLs).

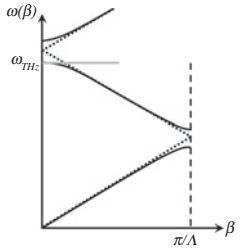


**Fig. 1** *Schematic dispersion curve of SPPs on metallic surface sculpted with second-order grating (solid line)*

Grey line: operating frequency; black dotted line: light line; black dashed line: boundary of first Brillouin zone

To what degree can one engineer the dispersion properties of SPPs? The asymptotic SPP frequency seems to be intrinsically determined by the materials' properties: by inserting a simplified Drude model $\varepsilon_m = 1 - \omega_p^2/\omega^2$ in the formula $\mathrm{Real}(\varepsilon_m) = -\varepsilon_d$, one obtains the asymptotic SPP frequency $\omega_{sp} = \omega_p/\sqrt{1+\varepsilon_d}$, where $\omega_p = \sqrt{Ne^2/(\varepsilon_0 m^*)}$ is the bulk plasma frequency; $e$, $m^*$, and $N$ are the elementary charge, the effective mass, and the density of the electrons, respectively. The expression for $\omega_p$ implies that the asymptotic SPP frequency can be tuned through changing $N$. One such approach is to, for example, use doped semiconductors, the carrier concentrations of which are much lower than those in metals and can be tuned by adjusting temperature or by other means [14–17].

A completely different method to engineer the SPP dispersion is to sculpt subwavelength features on metallic surfaces. It works by introducing localised electromagnetic modes strongly interacting with a structured surface, which significantly slows down the group velocity of SPPs and brings the asymptotic SPP frequency into the THz frequency range. Such microstructured surfaces are called designer plasmonic structures or 'spoof' SPP structures, as introduced by Pendry, Martín-Moreno, and García-Vidal [18, 19] and observed on structured metals at THz frequencies [20]. Interestingly, such structures were studied in the context of microwaves as early as the 1950s [21, 22] but have been largely unknown to the optics community.

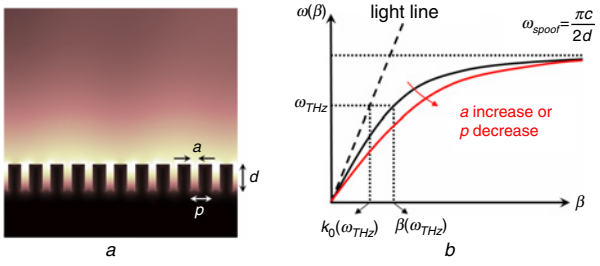


**Fig. 2** *Physics of spoof SPPs*

*a* Geometry of spoof SPP structure and schematic electric-field distribution
*b* Schematic dispersion diagram for THz spoof SPPs on corrugated surface of perfect electric conductor

Consider an array of grooves with subwavelength periodicity, $p$, sculpted on the surface of a perfect electric conductor; see Fig. 2*a*. The asymptotic frequency is given by [19]

$$\omega_{sp} = \pi c/2d \quad (3)$$

where $d$ is the groove depth, and $c$ the velocity of light in vacuum. Physically, (3) (or equivalently $d = \lambda_o/4$) corresponds to the first-order standing wave along the depth of the grooves: the phase accumulated during a roundtrip of the groove cavity mode is $2\pi$ (the wavevector times $2d$ contributes $\pi$, while the other $\pi$ originates from reflection of

the mode at the bottom of the grooves). An alternative way to understand (3) is to treat each groove as a waveguide shorted at the end. According to transmission line theory, the input impedance of such a terminated waveguide is [23]

$$\eta = i\eta_o \tan(k_o d) \tag{4}$$

where $d$, the groove depth, is now the length of the waveguide, and $\eta_o \sim 377\ \Omega$ is the free-space impedance. Equation (4) predicts that the impedance will be purely resistive if $d = \lambda_o/4$, while it will be inductive (capacitive) if $d < \lambda_o/4 (d > \lambda_o/4)$. Resistive impedance means that current and voltage are in phase and therefore net power will flow into the grooves and finally be dissipated through absorption. Physically, the accumulation of energy in the cavity grooves for $\omega$ near the asymptotic frequency $\omega_{sp}$ is the reason for the small group velocity.

Another type of spoof SPP structures comprises square indentations of side $a$ arranged on a $d \times d$ lattice sculpted on a metallic surface. The asymptote of the SPP dispersion is given by [18]

$$\omega_{sp} = \pi c/a$$

corresponding to the cutoff frequency of a square metallic waveguide of width $a$. Physically, SPPs with frequencies higher than $\pi c/a$ will couple into the waveguide modes.

Since $\omega_{sp}$ is not directly associated with the optical properties of the interface, as in the case of conventional SPPs, one can engineer the spoof SPP dispersion curve and obtain a sizeable deviation between the curve and the light line at the THz frequency of interest, i.e. $\beta(\omega_{THz}) > k_o(\omega_{THz})$ [18–20]; see Fig. 2*b*. As a result, the out-of-plane wavevector $\kappa(\omega_{THz})$ can be large, corresponding to confined SPPs with a $1/e$ decay distance in the air normal to the interface equal to $1/|\kappa|$ [20].

*Application of plasmonics in THz laser collimation:* We demonstrate the power of THz plasmonics by addressing one of the key problems in THz science and technology. We will show that collimators based on plasmonic second-order gratings combined with designer plasmonic structures can greatly improve the beam quality of THz QCLs.

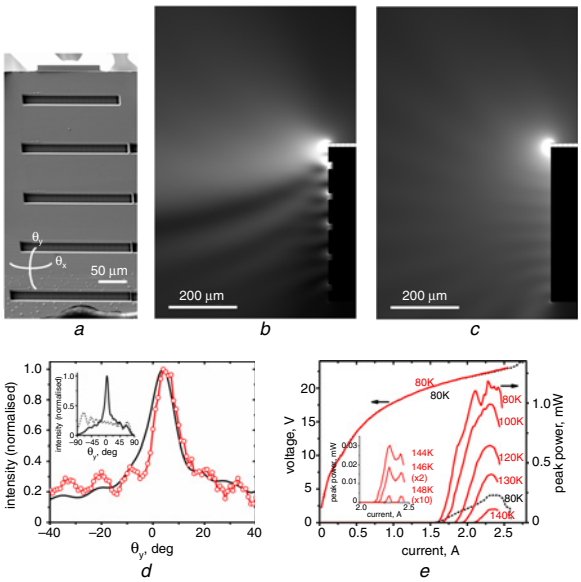


**Fig. 3** *Results for $\lambda_o = 100\ \mu m$ THz QCL with second-order-grating collimator directly sculpted into GaAs facet*

*a* SEM image of device facet
Laser waveguide 125 μm wide, 1.2 mm long on 450 μm-thick GaAs substrate (n-doped to $\sim 1.6 \times 10^{18}$ cm$^{-3}$). Grating has groove width and depth of 18 μm and 14 μm, respectively, and has periodicity of 88 μm. Centre-to-centre distance between laser aperture and nearest groove is 58 μm
*b*, *c* Simulated electric-field distribution (|E|) of device with second-order-grating collimator and of original device, respectively
*d* Red circles and black curve are measured and calculated vertical far-field emission of device, respectively
Insets: Calculated vertical far-field emission of original (dotted curve) and collimated (solid curve) devices
*e* Light output and voltage against pump current (*L-I-V*) characteristics and temperature performances of device before (black) and after (red) defining the collimator
Details on experimental setup and detection technique provided in [32]

THz QCLs have undergone rapid development recently and have significant potential for applications in sensing, imaging, and heterodyne detection of chemicals [24–27]. THz QCLs with the lowest threshold currents and the highest operating temperatures to date take advantage of the high optical confinement (near 100%) and heat removal properties of a microstrip waveguide design, in which the laser active core, about 10 μm thick, is sandwiched between a metal strip and a ground metal plane [28–30]. However, this design leads to a large impedance mismatch between the waveguide and free-space modes, which gives rise to inefficient power out-coupling and poor beam quality [29, 30]. For example, the power reflectivity of laser modes at the aperture is ~80–90% [31], and the laser emission is extremely divergent with a divergence angle ~180° perpendicular to the semiconductor layers, which represents a serious problem for efficient power collection.

To address these problems, we first adapted a design that is based on a plasmonic second-order grating [32], see Fig. 3*a*. The collimator works by coupling the waveguide laser mode to SPPs on the device facet and using the grating to scatter their energy coherently into the far field, thereby overcoming the diffraction limit set by the subwavelength aperture of the original laser. This is essentially an antenna array effect. All the grating grooves are sculpted directly into the GaAs facet using focused-ion beam (FIB) milling. We take advantage of the fact that in the THz regime GaAs is 'metallic' with the real part of its permittivity being negative for carrier concentrations of $n \sim 10^{17}$ cm$^{-3}$ and higher. The limited area of the facet allows only five grating grooves to be defined, see Fig. 3*a*. To enhance the interaction between the grating and the SPPs on the facet, we used fairly large grating grooves (depth and width ~15–20% of $\lambda_o$) so that the energy of the SPPs can be scattered into the far field as efficiently as possible. The effects of the second-order grating on the dispersion of SPPs are best illustrated by the improved SPP confinement; compare Figs. 3*b* and *c*.

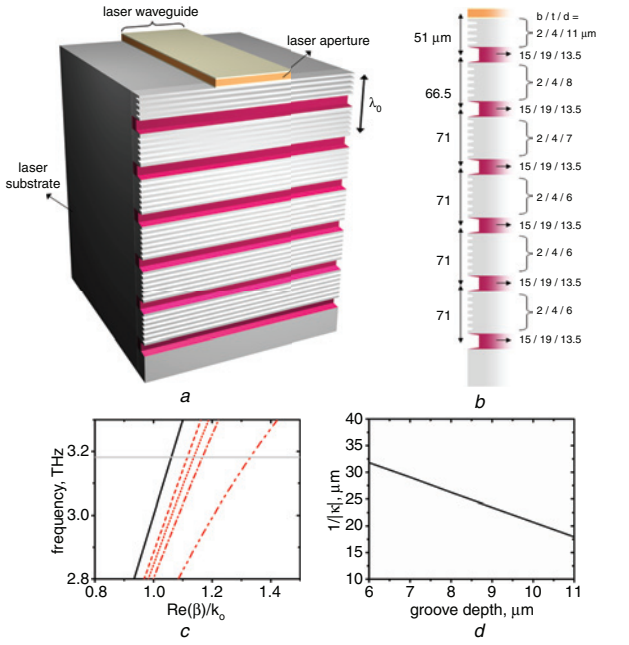


**Fig. 4** *Design of collimator consisting of second-order grating and spoof SPP grooves*

*a* Schematic of THz QCL integrated with collimator
*b* Cross-section of design for $\lambda_o = 94\ \mu m$ device
Width of bottom and top of grooves, and their depth are labelled as *b*, *t*, *d*, respectively. Period of spoof SPP grooves is 8 μm
*c* Black solid curve is dispersion diagram of Zenneck waves on planar semiconductor/air interface, which is very close to light line. Horizontal grey line indicates lasing frequency. Other curves are dispersion diagrams corresponding to different sections of spoof SPP structures. Dashed curve: $b/t/d = 2/4/6$ μm; dotted curve: $b/t/d = 2/4/7$ μm; dash-dotted curve: $b/t/d = 2/6/8$ μm; dash-double-dotted curve: $b/t/d = 2/4/11$ μm.
*d* $1/e$ decay length of spoof SPP electric field (|*E*|) normal to interface into air against *d*.

The measured vertical far-field emission profile of the device shows a full-width at half-maximum (FWHM) divergence angle of ~15°, which agrees reasonably well with simulation (Fig. 3*d*). Thanks to the improved emission profile, the collected power of the device increases by a factor of ~5 compared to the original unpatterned device at 80 K

(Fig. 3*e*). However, there is a fairly large background outside the central lobe, and this is due to the dominance of the direct emission from the laser aperture over the secondary emissions from the grating grooves. The latter are comparatively weak because of the inefficient coupling into the SPPs.

A greatly improved design involves adding spoof SPP grooves adjacent to the laser aperture and between the second-order grating grooves. A schematic of such a design for a ~3.19 THz ($\lambda_o = 94$ μm) laser and its cross-section are shown in Figs. 4*a* and *b*, respectively. Two colours are used in the Figures to identify the second-order grating (pink) and the spoof SPP grooves (blue).

At the aperture, the laser emits both directly into the far field and into SPPs on the device facet. In the original unpatterned device, both components have a wavevector close to $k_o$. The wavevector of the laser waveguide mode is several times larger, $\sim n_{eff}k_o$ ($n_{eff} \sim 3.5$ is the effective mode index). A wavevector mismatch then exists at the aperture between the laser waveguide mode, the SPP mode on the facet, and the free space mode. In our collimator, the spoof SPP grooves adjacent to the aperture increase the in-plane wavevector of the SPPs, reducing the wavevector mismatch. More light is therefore coupled out from the laser cavity and a larger percentage of it is channelled into the SPPs on the facet instead of being directly emitted into the far field. Most importantly, all the spoof SPP grooves on the facet greatly increase the confinement of SPPs to the surface, thus improving the scattering efficiency of the second-order grating. Constructive interference between the scattered waves and the direct emission from the laser aperture gives rise to a low-divergence beam normal to the facet in the far field.

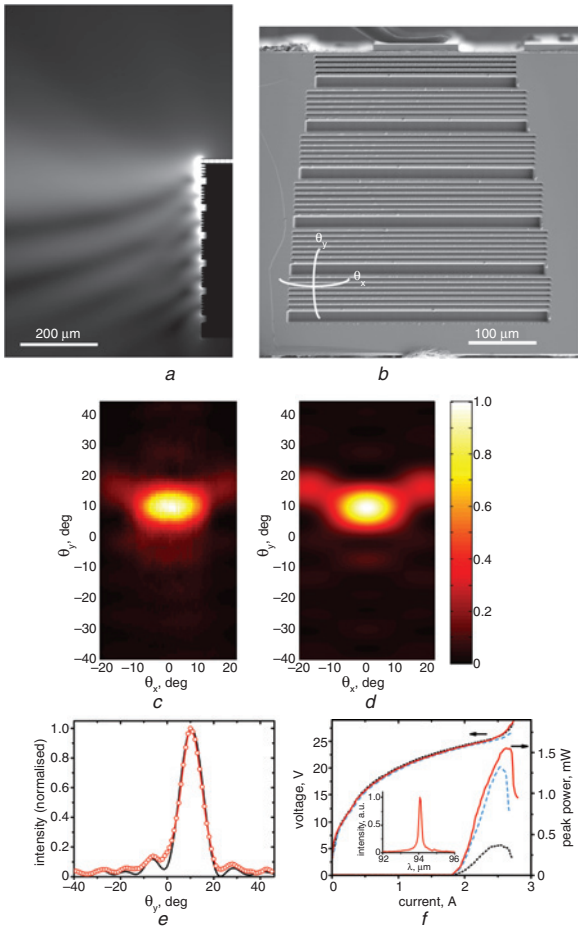


**Fig. 5** *Simulation and experimental results for collimator consisting of second-order grating and spoof SPP structures*

*a* Simulated electric field distribution (|E|) of device
*b* SEM image of device facet
Device emits at $\lambda_o = 94$ μm
*c*, *d* Measured and simulated emission patterns of device
*e* Vertical line-scans of (Fig. 5*c*) (circles) and (Fig. 5*d*) (solid curve) along $\theta_x = 0°$
*f* *L-I-V* characteristics of device
Dotted, dashed, and solid curves are for unpatterned device, device with only second-order grating and device with complete collimator, respectively
Inset: Spectrum of collimated device measured at $I = 2.5$ A

Fig. 4*c* shows that the in-plane wavevector increases by ~25% for the spoof SPP grooves adjacent to the laser aperture (dash-double-dotted curve). The depth of the spoof SPP grooves was chosen to be in the range 6–11 μm to provide sufficient confinement without introducing large optical losses, which are mainly due to absorption in the plasmonic medium and rise sharply as the groove depth increases [33]. Fig. 4*d* shows that the confinement of SPPs is improved to a few tens of micrometres, representing a reduction by approximately one order of magnitude compared to Zenneck waves on a planar interface (~300 μm).

The simulated electric-field distribution of the device is presented in Fig. 5*a*. Waves scattered from the laser facet by the collimator are clearly observed in the near and meso field, and confined spoof SPPs can be seen on the facet. Simulations indicate that compared to the original unpatterned device, the power throughput of the collimated device is increased by approximately 25%. In addition, it is estimated that about half of the laser output is coupled into SPP modes while the remaining half is emitted directly into the far field. In contrast, for the device with only the second-order grating, Fig. 3, the power coupled into SPPs is merely 15%, while the remaining 85% is radiated directly into the far field.

Fig. 5*b* shows an SEM image of the facet of a fabricated device. The collimator occupies a small footprint with dimensions $\sim 4\lambda_o \times 4.5\lambda_o$. The central beam has vertical and lateral FWHM divergence angles of ~11° and ~19°, respectively, in good agreement with the 3D full-wave simulation results; compare Figs. 5*c* and *d*. The optical background has average intensity below 10% of the central lobe peak intensity (Fig. 5*e*), owing to a more balanced direct emission from the aperture and secondary emissions from the facet. The beam quality of our collimated device is better than or comparable to those obtained in THz QCLs with higher-order gratings, photonic crystals, or mounted micro-optical elements [34–39]. The small divergence beam emitted from our device is compatible with the receiver front end of modern sub-millimetre heterodyne detection systems [40, 41].

The collected power of the collimated device increases by a factor of ~4.5 compared to the original unpatterned device; see Fig. 5*f*. The increase in power collection efficiency is ~3.7 for the device with only the second-order grating. This difference in measured power is primarily a result of the increased total power throughput originating from the reduced wavevector mismatch. Based on the far-field measurements, the power in the main lobe of the collimated device is about two times larger than that of the device with only the second-order grating. The maximum operating temperature of the patterned device is 140 K, the same as that of the original device. Fig. 5*f* shows that the lasing threshold did not change after defining the collimator.

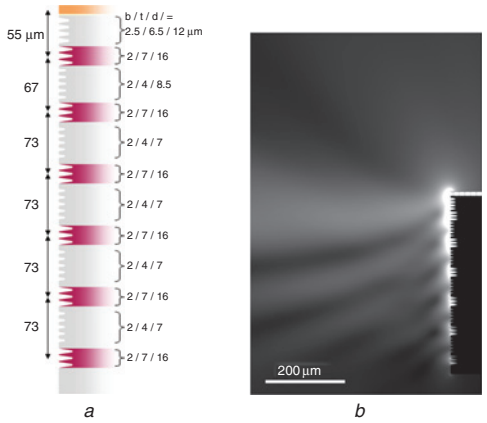


**Fig. 6** *Design and simulation for metasurface-based collimator*

*a* Cross-section of design for $\lambda_o = 100$ μm device
*b* Simulated electric field distribution (|E|) of device

We can go one step further to create a collimator consisting entirely of designer plasmonic structures by replacing the second-order grating in the last device with deep spoof SPP grooves [32]; see Fig. 6*a*. This seemingly minor change enables us to enter the metamaterial regime. Metamaterials have progressed rapidly in recent years, and their underlying paradigm is the design of spatial variations of the magnitude and sign of the refractive index so that the 'optical space' can be engineered in an almost arbitrary way to control electromagnetic waves [42–45]. Our design can be seen as an extension of the concept of metamaterials

to planar optics where the dispersion properties of SPPs are spatially tailored by structuring metallic surfaces. In this context 'metasurfaces' or 'metafilms' have found interesting applications such as subwavelength imaging [46], waveguiding [47, 48], phase masks [49], and the localisation [47, 48], confinement [50], and slowing of light [51].

The schematic of a metasurface-based collimator is shown in Fig. 6*a*. Spoof SPP grooves with different depths periodically modulate the dispersion of the SPPs on the device facet, effectively creating a second-order grating that couples the energy of the SPPs into the far field. The shallow 'light grey' grooves contribute to SPP confinement and fine tune the phase of the spoof SPPs to produce the maximum directivity. The 'light grey' grooves adjacent to the laser aperture help increase device power throughput by coupling more laser output into spoof SPPs on the facet. The fabricated device shows very similar performance as the previous one; see Fig. 7.

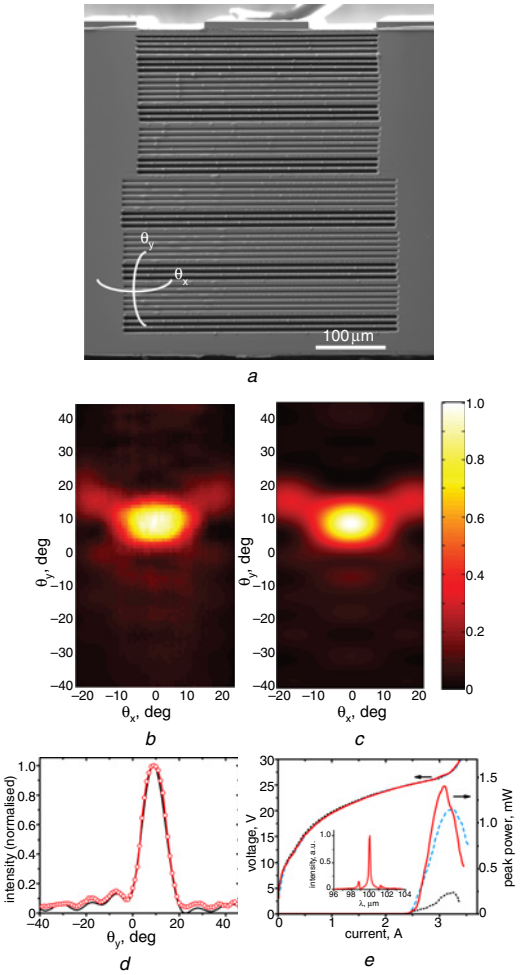


**Fig. 7** *Experimental results for $\lambda_o = 100$ μm QCL with metasurface-based collimator*

*a* SEM image of device facet
Device has 1.2 mm-long, 150 μm-wide, 10 μm-thick waveguide
*b*, *c* Measured and simulated emission profiles of device
*d* Line-scans of (Fig. 7*b*) (red circles) and (Fig. 7*c*) (solid curve) along $\theta_x = 0°$
*e* *L-I-V* characteristics of device
Dotted, dashed, and solid curves are for unpatterned device, device with only deep spoof SPP grooves and device with complete structure, respectively

Reduction of beam divergence occurs in both the vertical and lateral directions for the two devices presented above (Figs. 5 and 7). In the vertical direction, the collimation is explained by the antenna array effect. In the lateral direction, the collimation is due to an increased effective emission area; the spoof SPP patterns were intentionally fabricated to be much wider than the laser waveguide (see SEM images in Figs. 5*b* and 7*a*), which helps spread SPPs laterally. Physically, laser emission first excites the central section of the spoof SPP grooves; the electric field built up across the walls of the grooves will then propagate along the grooves in a way analogous to transverse electromagnetic (TEM) waves travelling along coplanar strip transmission lines. Simulations confirm that the lateral divergence is roughly inversely proportional to the width of the collimator pattern; see Fig. 8.

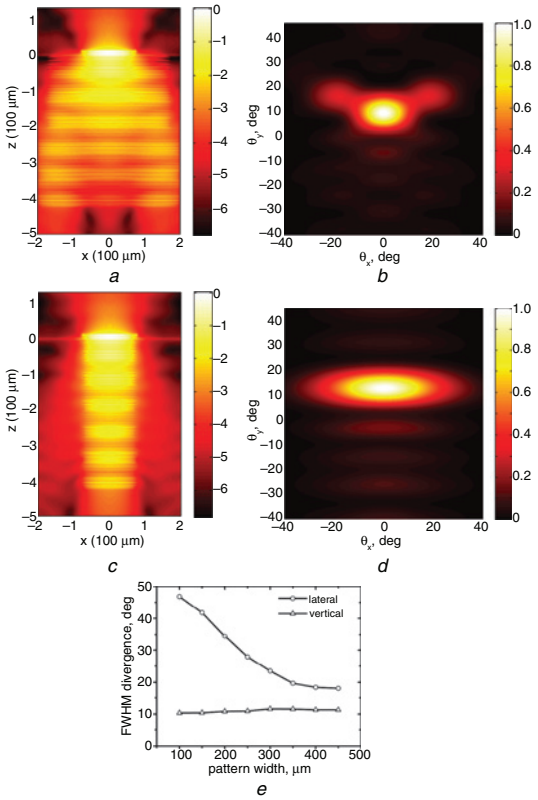


**Fig. 8** *Reducing lateral far-field divergence*

*a* Simulated near-field distribution ($\log_e(|E|/\max(|E|))$) for device in Fig. 7
Near field monitored on plane 1 μm above device facet
*b* Simulated far-field emission profile corresponding to near-field distribution in (Fig. 8*a*)
*c* Simulated near-field distribution of another device, collimator of which has narrower lateral dimensions
Collimator is ~400 μm wide in (Fig. 8*a*) but only 150 μm wide in (Fig. 8*c*); other design parameters are same
*d* Simulated far-field emission profile corresponding to near-field distribution in (Fig. 8*c*)
*e* Lateral and vertical far-field divergence against width of collimator

Our spoof SPP grooves, in a more strict sense, belong to channel waveguides that have been studied extensively in recent years [52–57]. Such waveguides support the so-called channel polaritons that propagate along the channel grooves and are well localised to the immediate vicinity of the grooves. Such polariton modes have larger effective mode index compared to SPPs on a planar interface. To calculate their dispersion properties, readers can refer to [52], which provides thorough theoretical studies of channel polaritons based on Green's second integral identity; in addition, [55–58] describe an effective-index method for semi-quantitative modelling of channel polaritons. We note that the channel grooves in our devices are closely spaced and therefore coupled, so calculating the properties of an isolated channel may not properly explain the physics of our structures. In fact, this coupling effect can be exploited to realise new functionalities; for example, [59] shows that in an array of coupled aperiodic metal-insulator-metal (MIM) waveguides, a guided mode is able to 'hop' from one waveguide to the next, leading to deep-subwavelength focusing and steering of light.

*Conclusion and perspective:* In summary, we have demonstrated that semiconductor microstructures can effectively tailor the dispersion properties of surface plasmon polaritons in the THz frequency range, and that the performance of THz QCLs can be significantly enhanced by monolithically integrating plasmonic structures on their facets.

Semiconductors are ideal media for THz plasmonics. First, owing to smaller carrier densities, the plasma frequency is much lower in semiconductors compared to that of metals. As a result, in the THz frequency range the confinement of SPPs to planar interfaces is largely improved, from typically centimetres for metals to a few hundred micrometres for semiconductors. Secondly, doped semiconductors offer great versatility

because their optical properties (e.g. permittivity, anisotropy) can be tuned by applying optical excitation, electrical potentials [15, 60], or magnetic fields [1, 16, 17], or by controlling the temperature [14, 17].

Functional THz systems can be built by exploiting the unique characteristics of semiconductors and the low-loss properties of metals in this frequency range. For example, we envision creating reconfigurable semiconductor switches, filters, and beam splitters for THz light, impedance adaptors based on spoof SPP structures, compact waveguide networks based on channel polaritons, sensors that bring THz SPPs in close contact with analytes, and tunable antennas or antenna arrays that facilitate communications between devices and free space.

Last but not least, though not a primary focus of this Letter, plasmonic devices capable of concentrating THz light into subwavelength spots will provide a wealth of possibilities to THz science and technology. There have been a few proposals and experimental demonstrations in this direction, employing plasmonic structures such as tapered metal wires [61], tapered coaxial [62] or parallel-plate [63] waveguides, and corrugated metal wires [64]. These structures will be of vital importance for THz high resolution imaging or spectroscopy and for exploring nonlinear THz effects.

*Acknowledgments:* We acknowledge funding from AFOSR under contract no. FA9550-09-0505-DOD, the EPSRC (UK), and the European Research Council programmes 'NOTES' and 'TOSCA'. M. A. Kats is supported by the National Science Foundation through a Graduate Research Fellowship. We gratefully acknowledge constructive and helpful discussions with R. Blanchard, C. Pflügl, L. Diehl and A. Belyanin. We thank N. Antoniou for assistance in FIB milling. We also acknowledge support from the National Science Foundation, Harvard Nanoscale Science and Engineering Center (NSEC), and the Center for Nanoscale Systems (CNS) at Harvard University. Harvard CNS is a member of the National Nanotechnology Infrastructure Network (NNIN). The computations in this Letter were run on the Odyssey cluster supported by the Harvard Faculty of Arts and Sciences (FAS) Sciences Division Research Computing Group.


*2 August 2010*
doi: 10.1049/el.2010.2131

N. Yu, Q.J. Wang, M.A. Kats, J.A. Fan and F. Capasso (*School of Engineering and Applied Sciences, Harvard University, Cambridge, Massachusetts 02138, USA*)

E-mail: nyu@fas.harvard.edu

S.P. Khanna, L. Li, A.G. Davies and E.H. Linfield (*School of Electronic and Electrical Engineering, University of Leeds, Leeds LS2 9JT, United Kingdom*)

Q.J. Wang: Current address is School of Electrical and Electronic Engineering and School of Physical and Mathematical Sciences, Nanyang Technological University, 50 Nanyang Avenue, Singapore 639798, Singapore

## References

1 Boardman, A.D.: 'Electromagnetic surface modes' (Wiley, New York, 1982)
2 Raether, H.: 'Surface plasmons on smooth and rough surfaces and on gratings' (Springer, Berlin, 1988)
3 Maier, S.A.: 'Plasmonics: fundamentals and applications' (Springer-Verlag, New York, LLC, 2007)
4 Barnes, W.L., Dereux, A., and Ebbesen, T.W.: 'Surface plasmon subwavelength optics', *Nature*, 2003, **424**, pp. 824–830
5 Ozbay, E.: 'Plasmonics: merging photonics and electronics at nanoscale dimensions', *Science*, 2006, **311**, pp. 189–193
6 Atwater, H.A.: 'The promise of plasmonics', *Sci. Am.*, 2007, **296**, (4), pp. 56–63
7 Mie, G.: 'Beiträge zur Optik trüber Medien, speziell kolloidaler Metallösungen', *Ann. Phys.*, 1908, **330**, pp. 377–445
8 Zenneck, J.: 'Über die Fortpflanzung ebener elektromagnetischer Wellen längs einer ebenen Leiterfläche und ihre Beziehung zur drahtlosen Telegraphie', *Ann. Phys.*, 1907, **23**, pp. 846–866
9 Sommerfeld, A.: 'Über die Ausbreitung der Wellen in der drahtlosen Telegraphie', *Ann. Phys.*, 1909, **28**, pp. 665–736
10 Stratton, J.A.: 'Electromagnetic theory' (McGraw-Hill Book Company, New York, 1941)
11 Kitson, S.C., Barnes, W.L., and Sambles, J.R.: 'Full photonic band gap for surface modes in the visible', *Phys. Rev. Lett.*, 1996, **77**, pp. 2670–2673
12 Weeber, J.-C., Lacroute, Y., Dereux, A., Devaux, E., Ebbesen, T., Girard, C., González, M.U., and Baudrion, A.-L.: 'Near-field characterization of Bragg mirrors engraved in surface plasmon waveguides', *Phys. Rev. B*, 2004, **70**, p. 235406
13 Gómez Rivas, J., Kuttge, M., Haring Bolivar, P., Kurz, H., and Sánchez-Gil, J.A.: 'Propagation of surface plasmon polaritons on semiconductor gratings', *Phys. Rev. Lett.*, 2004, **93**, p. 256804
14 Gómez Rivas, J., Kuttge, M., Kurz, H., Haring Bolivar, P., and Sánchez-Gil, J.A.: 'Low-frequency active surface plasmon optics on semiconductors', *Appl. Phys. Lett.*, 2006, **88**, p. 082106
15 Allen, J., Tsui, D.C., and Logan, R.A.: 'Observation of the two-dimensional plasmon in silicon inversion layers', *Phys. Rev. Lett.*, 1977, **38**, pp. 980–983
16 Kushwaha, M.S.: 'Plasmons and magnetoplasmons in semiconductor heterostructures', *Surf. Sci. Rep.*, 2001, **41**, pp. 1–416
17 Wang, X., Belyanin, A.A., Crooker, S.A., Mittleman, D.M., and Kono, J.: 'Interference-induced terahertz transparency in a semiconductor magneto-plasma', *Nature Phys.*, 2010, **6**, pp. 126–130
18 Pendry, J.B., Martín-Moreno, L., and García-Vidal, F.J.: 'Mimicking surface plasmons with structured surfaces', *Science*, 2004, **305**, pp. 847–848
19 García-Vidal, F.J., Martín-Moreno, L., and Pendry, J.B.: 'Surfaces with holes in them: new plasmonic metamaterials', *J. Opt. A: Pure Appl. Opt.*, 2005, **7**, pp. S97–S101
20 Williams, C.R., Andrews, S.R., Maier, S.A., Fernández-Domínguez, A.I., Martín-Moreno, L., and García-Vidal, F.J.: 'Highly confined guiding of terahertz surface plasmon polaritons on structured metal surfaces', *Nature Photonics*, 2008, **2**, pp. 175–179
21 Goubau, G.: 'Surface waves and their application to transmission lines', *J. Appl. Phys.*, 1950, **21**, pp. 1119–1128
22 Rotman, W.: 'A study of single-surface corrugated guides', *Proc. IRE*, 1951, **39**, pp. 952–959
23 Kong, J.A.: 'Electromagnetic wave theory' (EMW Publishing, Cambridge, 2000)
24 Hajenius, M., Khosropanah, P., Novenier, J.N., Gao, J.R., Klapwijk, T.M., Barbieri, S., Dhillon, S., Filloux, P., Sirtori, C., Ritchie, D.A., and Beere, H.E.: 'Surface plasmon quantum cascade lasers as terahertz local oscillators', *Opt. Lett.*, 2008, **33**, pp. 312–314
25 Kim, S.M., Hatami, F., Harris, J.S., Kurian, A.W., Ford, J., King, D., Scalari, G., Giovannini, M., Hoyler, N., Faist, J., and Harris, G.: 'Biomedical terahertz imaging with a quantum cascade laser', *Appl. Phys. Lett.*, 2006, **88**, p. 153903
26 Lee, A.W.M., Qin, Q., Kumar, S., Williams, B.S., Hu, Q., and Reno, J.L.: 'Real-time terahertz imaging over a standoff distance (>25 meters)', *Appl. Phys. Lett.*, 2006, **89**, p. 141125
27 Hübers, H.-W., Pavlov, S.G., Richter, H., Semenov, A.D., Mahler, L., Tredicucci, A., Beere, H.E., and Ritchie, D.A.: 'High-resolution gas phase spectroscopy with a distributed feedback terahertz quantum cascade laser', *Appl. Phys. Lett.*, 2006, **89**, p. 061115
28 Belkin, M.A., Wang, Q.J., Pflügl, C., Belyanin, A., Khanna, S.P., Davies, A.G., Linfield, E.H., and Capasso, F.: 'High-temperature operation of terahertz quantum cascade laser sources', *IEEE J. Sel. Top. Quantum Electron.*, 2009, **15**, pp. 952–967
29 Williams, B.S.: 'Terahertz quantum-cascade lasers', *Nature Photonics*, 2007, **1**, pp. 517–525
30 Scalari, G., Walther, C., Fischer, M., Terazzi, R., Beere, H., Ritchie, D., and Faist, J.: 'THz and sub-THz quantum cascade lasers', *Laser Photonics Rev.*, 2008, **3**, pp. 45–66
31 Kohen, S., Williams, B.S., and Hu, Q.: 'Electromagnetic modeling of terahertz quantum cascade laser waveguides and resonators', *J. Appl. Phys.*, 2005, **97**, p. 053106
32 Yu, N., Wang, Q.J., Kats, M.A., Fan, J.A., Khanna, S.P., Li, L., Davies, A.G., Linfield, E.H., and Capasso, F.: 'Designer spoof-surface-plasmon structures collimate terahertz laser beams', *Nature Mater.*, 2010, **9**, pp. 730–735
33 Wang, B., Liu, L., and He, S.: 'Propagation loss of terahertz surface plasmon polaritons on a periodically structured Ag surface', *J. Appl. Phys.*, 2008, **104**, p. 103531
34 Lee, A.W.M., Qin, Q., Kumar, S., Williams, B.S., Hu, Q., and Reno, J.L.: 'High-power and high-temperature THz quantum-cascade lasers based on lens-coupled metal-metal waveguides', *Opt. Lett.*, 2007, **32**, pp. 2840–2842
35 Amanti, M.I., Fischer, M., Walther, C., Scalari, G., and Faist, J.: 'Horn antennas for terahertz quantum cascade lasers', *Electron. Lett.*, 2007, **43**, pp. 573–574
36 Fan, J.A., Belkin, M.A., Capasso, F., Khanna, S., Lachab, M., Davies, A.G., and Linfield, E.H.: 'Surface emitting terahertz quantum cascade laser with a double-metal waveguide', *Opt. Express*, 2006, **14**, pp. 11672–11680

37 Mahler, L., Tredicucci, A., Beltram, F., Walther, C., Faist, J., Witzigmann, B., Beere, H.E., and Ritchie, D.A.: 'Vertically emitting microdisk lasers', *Nature Photonics*, 2009, **3**, pp. 46–49

38 Amanti, M.I., Fischer, M., Scalari, G., Beck, M., and Faist, J.: 'Low-divergence single-mode terahertz quantum cascade laser', *Nature Photonics*, 2009, **3**, pp. 586–590

39 Chassagneux, Y., Colombelli, R., Maineult, W., Barbieri, S., Beere, H.E., Ritchie, D.A., Khanna, S.P., Linfield, E.H., and Davies, A.G.: 'Electrically pumped photonic-crystal terahertz lasers controlled by boundary conditions', *Nature*, 2009, **457**, pp. 174–178

40 Gaidis, M.C., Pickett, H.M., Smith, C.D., Martin, S.C., Smith, R.P., and Siegel, P.H.: 'A 2.5-THz receiver front end for spaceborne applications', *IEEE Trans. Microw. Theory Tech.*, 2000, **48**, pp. 733–739

41 Siegel, P.H., and Dengler, R.J.: 'The dielectric-filled parabola: a new millimeter/submillimeter wavelength receiver/transmitter front end', *IEEE Trans. Antennas Propag.*, 1991, **39**, pp. 40–47

42 Engheta, N., and Ziolkowski, R.W.: 'Metamaterials: physics and engineering explorations' (Wiley-IEEE Press, 2006)

43 Cai, W., and Shalaev, V.M.: 'Optical metamaterials, fundamentals and applications' (Springer, 2009)

44 Pendry, J.B., Schurig, D., and Smith, D.R.: 'Controlling electromagnetic fields', *Science*, 2006, **312**, pp. 1780–1782

45 Leonhardt, U.: 'Optical conformal mapping', *Science*, 2006, **312**, pp. 1777–1780

46 Smolyaninov, I.I., Hung, Y.-J., and Davis, C.C.: 'Imaging and focusing properties of plasmonic metamaterial devices', *Phys. Rev. B*, 2007, **76**, p. 205424

47 Beermann, J., Radko, I.P., Boltasseva, A., and Bozhevolnyi, S.I.: 'Localized field enhancements in fractal shaped periodic metal nanostructures', *Opt. Express*, 2007, **15**, pp. 15234–15241

48 Radko, I.P., Volkov, V.S., Beermann, J., Evlyukhin, A.B., Sϕndergaard, T., Boltasseva, A., and Bozhevolnyi, S.I.: 'Plasmonic metasurfaces for waveguiding and field enhancement', *Laser Photonics Rev.*, 2009, **3**, pp. 575–590

49 Kanté, B., Lourtioz, J.-M., and de Lustrac, A.: 'Infrared metafilms on a dielectric substrate', *Phys. Rev. B*, 2009, **80**, p. 205120

50 Navarro-Cía, M., Beruete, M., Agrafiotis, S., Falcone, F., Sorolla, M., and Maier, S.A.: 'Broadband spoof plasmons and subwavelength electromagnetic energy confinement on ultrathin metafilms', *Opt. Express*, 2009, **17**, pp. 18184–18195

51 Gan, Q., Fu, Z., Ding, Y.J., and Bartoli, F.J.: 'Ultrawide-bandwidth slow-light system based on THz plasmonic graded metallic grating structures', *Phys. Rev. Lett.*, 2008, **100**, p. 256803

52 Novikov, I.V., and Maradudin, A.A.: 'Channel polaritons', *Phys. Rev. B*, 2002, **66**, p. 035403

53 Gramotnev, D.K., and Pile, D.F.P.: 'Single-mode subwavelength waveguide with channel plasmon-polaritons in triangular grooves on a metal surface', *Appl. Phys. Lett.*, 2004, **85**, p. 6323

54 Bozhevolnyi, S.I., Volkov, V.S., Devaux, E., Laluet, J.-Y., and Ebbesen, T.W.: 'Channel plasmon subwavelength waveguide components including interferometers and ring resonators', *Nature*, 2006, **440**, p. 508

55 Bozhevolnyi, S.I., Volkov, V.S., Devaux, E., and Ebbesen, T.W.: 'Channel plasmon-polariton guiding by subwavelength metal grooves', *Phys. Rev. Lett.*, 2005, **95**, p. 046802

56 Bozhevolnyi, S.I.: 'Effective-index modeling of channel plasmon polaritons', *Opt. Express*, 2006, **14**, pp. 9467–9476

57 Bozhevolnyi, S.I., and Jung, J.: 'Scaling for gap plasmon based waveguides', *Opt. Express*, 2008, **16**, pp. 2676–2684

58 Hocker, G.B., and Burns, W.K.: 'Model dispersion in diffused channel waveguides by the effective index method', *Appl. Opt.*, 1997, **16**, pp. 113–118

59 Verslegers, L., Catrysse, P.B., Yu, Z., and Fan, S.: 'Deep-subwavelength focusing and steering of light in an aperiodic metallic waveguide array', *Phys. Rev. Lett.*, 2009, **103**, p. 033902

60 Chen, H.-T., Padilla, W.J., Zide, J.M.O., Gossard, A.C., Taylor, A.J., and Averitt, R.D.: 'Active terahertz metamaterial devices', *Nature*, 2006, **444**, pp. 597–600

61 Astley, V., Mendis, R., and Mittleman, D.M.: 'Characterization of terahertz field confinement at the end of a tapered metal wire waveguide', *Appl. Phys. Lett.*, 2009, **95**, p. 031104

62 Rusina, A., Durach, M., Nelson, K.A., and Stockman, M.I.: 'Nanoconcentration of terahertz radiation in plasmonic waveguides', *Opt. Express*, 2008, **16**, pp. 18576–18589

63 Zhan, H., Mendis, R., and Mittleman, D.M.: 'Superfocusing terahertz waves below $\lambda/250$ using plasmonic parallel-plate waveguides', *Opt. Express*, 2010, **18**, pp. 9643–9650

64 Maier, S.A., Andrews, S.R., Martín-Moreno, L., and García-Vidal, F.J.: 'Terahertz surface plasmon-polariton propagation and focusing on periodically corrugated metal wires', *Phys. Rev. Lett.*, 2006, **97**, p. 176805